Photocatalytic Generation of Oxygen Radicals by the Water-Soluble Bacteriochlorophyll Derivative WST11, Noncovalently Bound to Serum Albumin

Idan Ashur,[†] Ruth Goldschmidt,[†] Iddo Pinkas,[†] Yoram Salomon,[‡] Grzegorz Szewczyk,[§] Tadeusz Sarna,[§] and Avigdor Scherz*[,†]

Department of Plant Sciences, The Weizmann Institute of Science, Rehovot, Israel, Department of Biological Regulation, The Weizmann Institute of Science, Rehovot, Israel, and Department of Biophysics, Jagiellonian University, Krakow, Poland

Received: January 20, 2009; Revised Manuscript Received: May 5, 2009

Light-induced radical generation is the hallmark of fundamental processes and many applications including photosynthesis and photodynamic therapy (PDT). In this manuscript, we present two novel observations made upon monitoring light-induced generation of reactive oxygen species (ROS) in aqueous solutions by WST11, a water-soluble derivative of the photosynthetic pigment Bacteriochlorophyll *a* (Bchl). Using a host of complementary experimental techniques including time-resolved spectroscopy at the subpicosecond to the millisecond range, ESR spectroscopy, electrochemistry, spectroelectrochemistry, oximetry, and protein mass spectroscopy, we first show that in aqueous solutions WST11 generates only superoxide ($O_2^{-\bullet}$) and hydroxyl ($OH^{\bullet}$) radicals with no detectable traces of singlet oxygen. Second, we show that WST11 makes a noncovalent complex with human serum albumin (HSA) and that this complex functions as a photocatalytic oxidoreductase at biologically relevant concentrations enabling approximately 15 cycles of electron transfer from the associated HSA protein to molecular oxygen in the solution. These findings rule out the paradigm that porphyrin and chlorophyll based PDT is mainly mediated by formation of singlet oxygen, particularly in vascular targeted photodynamic therapy (VTP) with sensitizers that undergo photoactivation during circulation in the plasma, like [Pd]-Bacteriopheophorbide (WST09, Tookad). At the same time, our findings open the way for new design paradigms of novel sensitizers, since $O_2^{-\bullet}$ and $OH^{\bullet}$ radicals are well-recognized precursors of important pathophysiological processes that can be activated for achieving tumor eradication. Moreover, the finding that promiscuous protein scaffolds become sinks for holes and electrons when holding light-activated pigments provides a new insight to the evolution and action mechanism of natural light activated oxidoreductases (such as photosynthetic reaction centers) and new guidelines for the preparation of synthetic-light converting machineries.

Introduction

Photoexcitation of pigment molecules followed by energy transfer and radical generation promotes both constructive and destructive biological processes. The first group includes fundamental biological machineries such as photosynthesis and vision, while photoinhibition and plants senescence are two examples of the second group. The photocatalytic centers involved in the constructive processes usually comprise protein scaffolds which hold the pigment molecules in a manner that assures unidirectional and well-controlled transfer of energy or electrons from donors to acceptors. The protein involvement in these processes has been thoroughly studied but remained controversial to date.[1,2] Light-induced destructive processes are usually the result of conformational changes or even disintegration of the pigment/protein complexes resulting in noncontrolled energy or electron transfer from the photoactive pigments into acceptor molecules that become highly active and impair vital cellular or tissue activities. An example is provided by the formation of reactive oxygen species (ROS) through energy or electron transfer from a host of photoexcited pigment molecules (sensitizers) into colliding or nearby molecular oxygen. This phenomenon was found responsible for photoinhibition[3] and several pathologies (e.g., porphyria)[4] and has been translated into a cancer treatment modality termed photodynamic therapy (PDT).[5] In PDT, pigments that can generate ROS at high yield upon illumination in the VIS−NIR wavelength range are delivered to a cancerous tissue and locally illuminated. The formed ROS initiate a cascade of events that result in reduction or oxidation of vital components (e.g., proteins and lipids) in the cellular compartment of the cancerous tissue and thereby cause cell death and tumor eradication. Numerous studies have suggested that the PDT toxicity in the cells is mainly mediated by singlet oxygen which dominates the ROS profile (type II mechanism).[6−9] In the type II mechanism, the photosensitizer in the excited triplet state can interact with ground state oxygen molecules, generating singlet oxygen through an energy transfer process.[10,11] An alternative route is the type I mechanism in which the photosensitizer in the excited triplet state can interact directly with the substrate and/or solvent through electron or proton transfer processes. This leads to generation of charged or neutral radicals, which quickly react with oxygen molecules to produce ROS such as superoxide ($O_2^{-\bullet}$) and hydroxyl ($OH^{\bullet}$) radicals and hydrogen peroxide (H_2O_2). Evidence for the

* Corresponding author. Tel.: +972-8-9342336. Fax: +972-8-9344181. E-mail: avigdor.scherz@weizmann.ac.il.
[†] Department of Plant Sciences, The Weizmann Institute of Science.
[‡] Department of Biological Regulation, The Weizmann Institute of Science.
[§] Jagiellonian University.

10.1021/jp900580e CCC: $40.75 © 2009 American Chemical Society
Published on Web 06/22/2009

SCHEME 1: Water-Soluble [Pd]-Bacteriopheophorbide Derivative, WST11

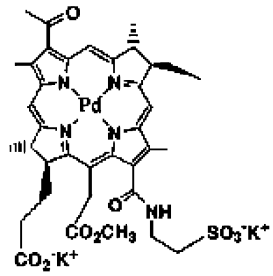

occurrence of the type I mechanism is limited and less conclusive.[10,11]

A new approach to PDT termed vascular-targeted PDT (VTP) aims to induce instantaneous collapse of the tumor vasculature. The consequent deprivation of nutrients and oxygen results in cell death and tumor eradication. So far, VTP has been applied using hydrophobic sensitizers that preferentially reside in the endothelial cells of the tumor vasculature during illumination and generate singlet oxygen.[12,13] Recently we developed a different approach to VTP using a novel class of amphiphilic photosensitizers comprising different derivatives of Bacteriochlorophyll *a* (Bchl).[14−17] These sensitizers stay in the circulation until clearance with minimal or even no uptake by the endothelial cells during illumination. Hence, ROS generation is confined to the aqueous plasma, resulting in instantaneous clot formation, vascular arrest, and high rates of tumor control, both in the preclinical[14,16−18] and clinical[19−22] arenas. We have previously hypothesized that under these conditions the ROS generation profile can be markedly different from the one assumed for the cellular environment[23] because the high dielectric nature of aqueous solutions may help promote electron transfer. Indeed, Vakrat-Haglili et al.[24] showed a dramatic increase in the content of $O_2^{-\bullet}$ and $OH^\bullet$ radicals when [Pd]-Bacteriopheophorbide (WST09, Tookad) was photoexcited in aqueous compared to organic solutions. However, the significant concentration of singlet oxygen still present in the aqueous solutions prevented a clear conclusion concerning the role played by the oxygen radicals in mediating the VTP effect. This important issue can now be resolved using the water-soluble [Pd]-Bacteriopheophorbide derivative (WST11, Stakel, Scheme 1)[14,16] that was recently synthesized by our lab in collaboration with Steba laboratories, France.

This compound has entered phase I/II clinical trials for AMD management[17] and localized prostate cancer. Unlike WST09, WST11 needs no micelles when being introduced to aqueous solutions. It stays in the plasma until clearance,[25] most probably as a noncovalent complex with human serum albumin (HSA),[14] and does not seem to primarily interact with endothelial cells.[17] Therefore, WST11 provides the means for studying the impact of ROS generation in the aqueous vascular lumen. Following this presumption, we set out to explore the generation of ROS by WST11 upon photoexcitation in stepwise reconstituted blood solutions, starting in buffered aqueous solutions and then adding different serum proteins, plasma, blood cells, etc. The present paper focuses on the effect of HSA on the ROS generation profile by photoexcited WST11 in aqueous solutions. Collectively, our data introduce a novel concept, suggesting that a noncovalent WST11−HSA complex acts as a light-activated oxido-reductase that catalyzes electron transfer from the protein matrix to the dissolved oxygen molecules, thereby amplifying the production of $O_2^{-\bullet}$ and $OH^\bullet$ radicals. Using optical absorption and fluorescence spectroscopy at the different time domains, spectroelectrochemistry, spin-trap ESR technique, dissolved oxygen concentration measurements, and gel electrophoresis techniques, we (1) followed the physical and chemical response of WST11 to photoexcitation in the presence of HSA and quenchers; (2) identified and quantified the evolved ROS; (3) monitored the rate and yield of oxygen consumption in response to photoexcitation of WST11 in the absence and presence of HSA; and (4) monitored induced chemical modifications of the HSA molecules subsequent to the ROS generation. We showed that in pure aqueous solutions (H_2O and D_2O) WST11 rapidly degrades through oxidative processes. The ROS profile comprises comparable amounts of $O_2^{-\bullet}$ and $OH^\bullet$ radicals (spin-trapped by DMPO and DEPMPO) but no detectable singlet oxygen. In the presence of HSA, the photochemical degradation of WST11 is profoundly retarded. Only $OH^\bullet$ radicals can be detected, and their total concentration increases by more than 2-fold compared with that observed in the absence of HSA. The rate and yield of oxygen consumption increases by more than an order of magnitude per single molecule of WST11. Upon adding the metal chelator desferrioxamine (DFO) to both HSA-free and HSA-containing solutions, a strong ESR signal of the trapped $O_2^{-\bullet}$ radical replaces that of the $OH^\bullet$ radical, suggesting that $O_2^{-\bullet}$ is the primarily formed ROS and the precursor of the $OH^\bullet$ radicals. Finally, upon the complete degradation of the WST11 reservoir, each HSA molecule appears to undergo peroxidation and, possibly, covalent binding to photodegradation products of the WST11 molecules.

Altogether, our findings establish the foundation for resolving the in vivo activity of WST11−VTP and may provide a new insight to the role played by the protein scaffold in light-induced electron transfer. In a photosystem II reaction center (PSII RC), a photoexcited pair of chlorophyll (Chl) molecules (termed P680) that are noncovalently bound to the protein scaffold transfers an electron through a chain of redox centers to a quinone molecule at the other side of the photosynthetic membrane. By oxidizing a nearby tyrosine (Tyr) residue, P680 is rapidly regenerated. Although the exceptionally high midpoint potential of the $P680/P680^+$ redox couple (+1.25 V) matches nicely that of the Tyr/Tyr^+ redox couple (+1.21 V),[26] the energetic barrier should be greatly reduced by an accompanied proton translocation from the $Tyr^{+\bullet}$ residue to form the more stable tyrosyl radical ($Tyr^\bullet$). This is possible in a protein scaffold having a nearby protonated side chain within a hydrogen bonding distance of the oxidizable Tyr.[27] Following these insights, Kalman et al.[28] were able to demonstrate $P860^+$ reduction in RC of purple bacteria by Tyr residues that replaced Arginine L135 and Arginine M164 although the $P860^+/P860$ midpoint potential is only +0.50 V. Thus, it appears that the protein milieu overcomes the midpoint potentials difference in a fashion that involves particular arrangement and interactions of amino acid residues. However, data shown in our present study suggest that a promiscuous protein scaffold can function as a nonspecific supplier of electrons when bound to Bchls and thereby facilitate their regeneration after oxidation. This finding may provide new guidelines for deciphering the evolution of photocatalytic protein−pigment complexes and constructing artificial systems for light energy conversion.

Materials and Methods

Different concentrations of WST11 solutions (Steba Biotech, stored as dry powder) were prepared in D-Phosphate Buffer Saline solution (PBS × 10, pH 7.4, Gibco) as specified for each experiment. 5,5-Dimethyl-1-pyrroline *N*-oxide (DMPO, GC

grade >97%), 2,2,6,6-tetramethyl-1-piperidone-*N*-oxyl (95%, 4-oxo-TEMP), desferrioxamine mesylate salt (95% TLC powder), and Albumin from Human Serum (essentially fatty acid free, lyophilized powder) were purchased from Sigma-Aldrich. 5-Diethoxyphosphoryl-5-methyl-1-pyrroline *N*-oxide (DEPMPO, 99.9% HPLC) was purchased from Calbiochem.

Electron-Spin Resonance Spectroscopy (ESR). Standard ESR measurements were carried out using a Magnettech ESR Miniscope MS 100 spectrometer, equipped with a Microwave X-band Bridge. The spectrometer operates at 9.3−9.55 GHz and 20 mW microwave power. The light source for the experiments was a Spectra Physics model 3900 Ti:sapphire laser (Spectra-Physics, Mountain View, California, USA), 1 W, pumped by 5 W of a 532 nm Spectra Physics Millenia Pro 10 W CW Nd:VO_4 laser. For the purpose of our experiments, the laser operated at 755 nm, and the input power was adjusted to 20 mW using neutral density optical filters. The sample was illuminated by an optical fiber that was located inside the ESR cavity and directed at the sample. This allowed simultaneous illumination and ESR detection. The produced $O_2^{-\bullet}$ and $OH^{\bullet}$ radicals were detected as the spin adducts DMPO−OOH and DMPO−OH, respectively. To verify if the DMPO−OH (or part of it) originates from DMPO−OOH degradation, we added 10% DMSO as a quencher of the $OH^{\bullet}$ radical.[29]

Optical Absorption Measurements. ***Steady-State and Submicro to the Millisecond Time Domain Measurements.*** Steady-state optical absorption spectra were recorded by a Thermo Scientific-Evolution 300 UV−visible spectrophotometer. Submicro to the millisecond time domain absorption measurements and luminescence measurements were performed as previously described.[24]

Time-Resolved Measurements at the Femtosecond to Picosecond Time Domain. The femtosecond laser system consists of several commercially available components. The system is driven by a mode-locked Ti:sapphire oscillator (Spectra Physics Tsunami) pumped by a CW diode pumped Nd:YVO4 laser (Millennia X). The oscillator produces a train of <100 fs pulses (bandwidth ∼10 nm fwhm), with a peak wavelength at around 815 nm, typically of 850 mW, corresponding to ∼10 nJ per pulse. The weak oscillator pulses are amplified by a chirped pulse regenerative amplifier (CPA) (Spectra Physics Spitfire). The pulses are first stretched to about 200 ps, then regeneratively amplified in a Ti:sapphire cavity, pumped by a pulsed Nd:YLF laser (Spectra Physics Evolution-15 operating at 1 kHz). After the pulse has been amplified and recompressed, its energy is about 1.0 mJ in a train of 1 kHz pulses. An independent pump pulse is obtained by pumping an optical parametric amplifier (Spectra Physics OPA-800CF) that produces 120 fs pulses tunable from 300 nm to 3 μm.

The output power of the OPA ranges from a few microjoules to tens of microjoules (depending on the chosen wavelength) at 1 kHz. The pump beam is mechanically chopped at half the amplifier repetition rate. The chopper (C-995 TTI) is synchronized to the Spitfire amplifier. Normally a few thousand pulse pairs are averaged to produce a transient absorption spectrum with a noise level below 0.3 mOD.

A small portion of the remaining amplified pulse is used to generate a white light continuum as a probe pulse. To this end, the Ti:sapphire beam is focused onto a 3 mm thick sapphire disk by a 10 cm focal length lens, and the numerical aperture of the beam is controlled by an iris placed in front of the lens, which helps to obtain a stable and smooth white light continuum (Riedle, E., private communication). The resulting beam is passed through a short pass filter to remove the remains of the fundamental beam from the white light continuum.

The pump and probe pulses are crossed in the sample at a small angle, while maintaining a magic angle between the pump and probe polarizations. The remains of the pump pulse are removed by an iris, and the probe light is imaged onto an optical fiber that brings it into an imaging interface that focuses the light onto the entrance slit of a Jobin Yivon Triax 180 spectrograph. The light is normally dispersed by a 300 1/mm grating onto a fast CCD camera (Andor Newton DU-970N-UV, operating at 1000 spectra per second using "crop mode"). The whole setup is controlled by a PC running National Instruments LabView. The time domain is scanned by delaying the pump pulse relative to the probe pulse using a hollow retroreflector mounted on a motorized translation stage (Aerotech, ALS130).

Gel Electrophoresis. Sodium dodecyl sulfate polyacrylamide gel−electrophoresis (SDS−PAGE) was performed using 1% polyacrylamide separating gel and 10% polyacrylamide stacking gel. Samples were diluted in a sample buffer, and the reference was the dual-color (Bio-Rad).

ESI−MS. Prior to mass spectrometry analysis, the samples were filtered in PD-10 columns (Sephadex G-25) and desalted using Porous R1 resin (ABI, Framingham, USA). The resin was equilibrated with 10 μL of 5% formic acid. An amount of 5 μL of the sample was applied to the R1 desalting column and washed with 5 μL of 5% formic acid three times. The samples were eluted by 50% methanol (MeOH) and 5% formic acid.

Human serum albumin mass spectra were acquired on an API 300 triple quadrupole mass spectrometer (ABI, Sciex, Concord, Ontario) using a nanoelectrospray ion source (Protana A/S, Denmark).

Molecular weight was determined by Analyst 1.4 software through the deconvolution of the multiply charged ions obtained after scanning the first quadrupole (Q1), operating in the positive mode. The typical ion source parameters are as follows: ion spray voltage 1.5kV, declustering potential (DP) 80 V, focusing potential (FP) 380 V, entrance potential (EP) 10 V, deflector −100 V, channel electron multiplier (CEM) 2700 V.

Electrochemical and Spectroelectrochemical Measurements. ***Cyclic Voltammetry (CV) Measurements.*** Cyclic voltammetry (CV) of WST11 (1.4×10^{-4} M) in acetonitrile (AN) was measured by using a three-electrode configuration at 25 °C. The working electrode was an Au electrode (1.6 mm diameter, BAS), and the counter electrode was a platinum wire. Potentials were measured vs Ag/Ag^+ reference electrode (BAS, 0.1 M $AgNO_3$, 0.6 V vs NHE). Supporting electrolyte was 0.1 M tetrabutlyammoniumfluoroborate (TBAF). Previous to each measurement, the working electrode was polished by the BAS polishing kit followed by several minutes of sonication in double distilled water and a thorough washing with methanol and electrolyte solutions.

Spectroelectrochemical Measurements. Spectroelectrochemical measurements of WST11 in AN were performed in a specially designed cell (optical path length of 500 μm) that was fitted to the cuvette holder of a Thermo Evolution 300 UV−VIS−NIR spectrophotometer. A transparent indium titanium oxide slide (ITO, sigma-Aldrich) served as the working electrode and a platinum wire as the auxiliary electrode. Potentials were measured vs a thin Ag/Ag^+ reference electrode (custom-made, 0.1 M $AgNO_3$, 0.6 V vs NHE). The ITO slide and the Pt wire were attached to electrical connectors that were mounted to a Teflon cover. The reference electrode and a thin tube (2 mm diameter, used for N_2 purging) were inserted into

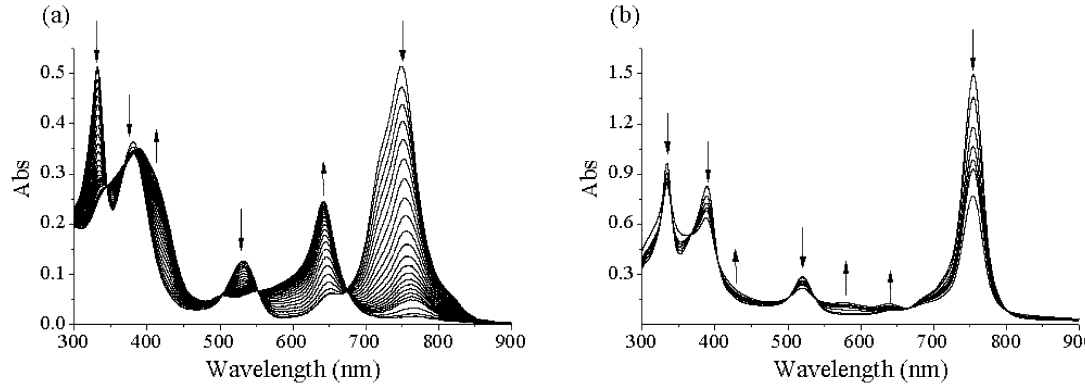

Figure 1. Photodegradation of 25 μM WST11 solutions under illumination at 755 nm (20 mW) for 10 min in (a) PBS and (b) PBS + 500 μM HSA.

the solution through dedicated apertures in the Teflon cover. The sample solutions were thoroughly degassed by N_2 for 30 min. To maintain anaerobic conditions, a moderate gas flow was maintained within the cuvette on top of the solution. The supporting electrolyte was 0.1 M tetrabutlyammoniumfluoroborate (TBAF). Monocationic and monoanionic species of WST11 were electrochemically generated by setting constant oxidative or reductive potentials (+600 and −1100 mV vs NHE, respectively). The measurements were performed at 25 °C.

Dissolved Molecular Oxygen Measurements. Oximetry measurements were performed by an ISO_2 dissolved oxygen sensor (Clark type, 2 mm diameter, World Precision Instruments). The electrode tip was inserted into the spectroscopic cuvette through an appropriate aperture, allowing concomitant monitoring of dissolved oxygen concentration and optical UV−VIS−NIR absorption.

Fluorescence Analysis. Fluorescence analysis was performed using a Cary Eclipse Fluorescence Spectrophotometer from Varian (Australia, Pty Ltd.). Samples were analyzed using a quartz cuvette. The results represent the mean of five measurements.

Results

Spectral Changes of WST11 in Aqueous Solutions, In Response to Continuous VIS−NIR Illumination. Figure 1 illustrates the response of WST11 in different solutions to continuous illumination at 755 nm.

The UV−VIS−NIR spectra of [M]−Bchls are composed of four well-resolved transition bands,[30−33] designated in order of increasing energy as Q_y, Q_x, B_x, and B_y (the x and y captions assign the symmetry axis along the pi system of the Bchl molecule). In PBS solution (Figure 1a), the four transitions are located at 750, 530, 390, and 340 nm, respectively. Upon illumination, these transition bands rapidly bleach, whereas new transitions at 647 and 410 nm emerge. These two transition bands are typical to chlorines the oxidized form of [Pd]-substituted Bchls,[24] indicating that WST11 undergoes photo-oxidation upon illumination. Under anaerobic conditions, this process does not occur, as implied by the stability of the corresponding optical absorption spectrum (data not shown). Addition of HSA to the aerobic solution greatly retards the photo-oxidation process (Figure 1b). Moreover, the photochemical products are different, presenting very weak absorption in the VIS region with a maximum at 580 nm. Importantly, at the working concentration of WST11 (25 μM), the Q_y transition undergoes broadening and exciton splitting, typical of Bchl aggregates.[34−36] These aggregates undergo monomerization upon adding HSA, and the excitonic transitions collapse as depicted by Figure 1b, consistent with our previous report.[14]

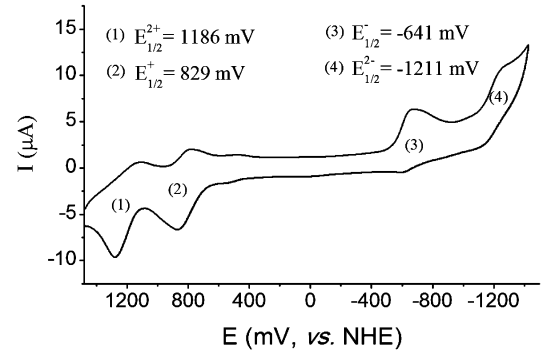

Figure 2. Cyclic voltammetry measurement of WST11 (500 μM) in aerated AN recorded at a scan rate of 75 V/s. The four detectable waves and the corresponding half-wave potential values are indicated and reported vs NHE. The positive half-wave potentials, designated as $E^{+}_{1/2}$ and $E^{2+}_{1/2}$, refer to the first and second oxidation of the Bchl pi system, respectively (formation of cation radical and dication species). The negative half-wave potentials, designated as $E^{-}_{1/2}$ and $E^{2-}_{1/2}$, refer to the first and second reduction of the pi system, respectively (anion radical and dianion species).

Electrochemistry and Spectroelectrochemistry of WST11. Figure 2 shows the CV response of WST11 in AN under anaerobic conditions.

The voltammogram features four quasi-reversible ring-centered (ring-centered refers to oxidation or reduction of the Bchl pi system as opposed to metal-centered reactions that occur on the central metal) oxidation waves.[37] The half-wave potentials of the mono- and dication species (mono- and dication species are products of first and second ring-centered oxidation processes, respectively) are 484 and 841 mV vs NHE, respectively. The half-wave potentials of the mono- and dianion species are −986 and −1556 mV vs NHE, respectively. The oxidation potentials of WST11 are less positive by ~100 mV than the corresponding oxidation potentials of previously characterized [M]−Bchl compounds.[37,38] In this respect, this finding implies that WST11 can be oxidized more easily then the WST09 derivative and therefore provides favorable thermodynamic conditions for the formation of the $O_2^{-\bullet}$ radical.

Figure 3 depicts the spectral changes introduced by the reversible and irreversible products of one-electron electrochemical oxidation and reduction of WST11 in AN under anaerobic conditions. Figure 3a shows the difference spectra of neutral WST11 and its electrochemical products obtained under a mono-oxidizing or reducing potential. Notably, the Q_y and Q_x of WST11 in AN are blue-shifted relative to their

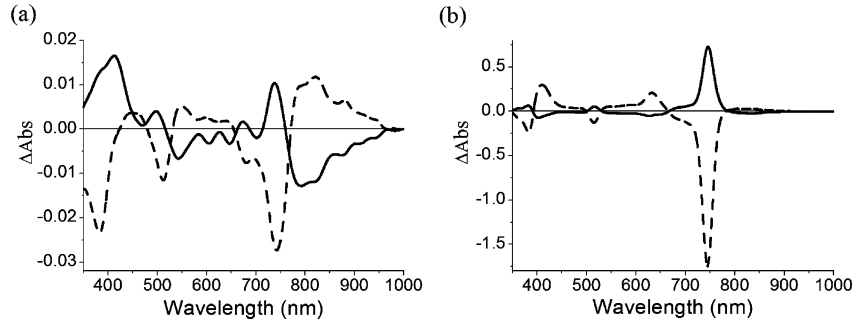

Figure 3. Difference spectra of neutral WST11 and its electrochemically produced species: (a) dashed line, difference of neutral and mono-oxidized species; solid line, difference of mono-oxidized and back-reduced species; (b) dashed line, difference of neutral and monoreduced species; solid line, difference of monoreduced and back-oxidized species.

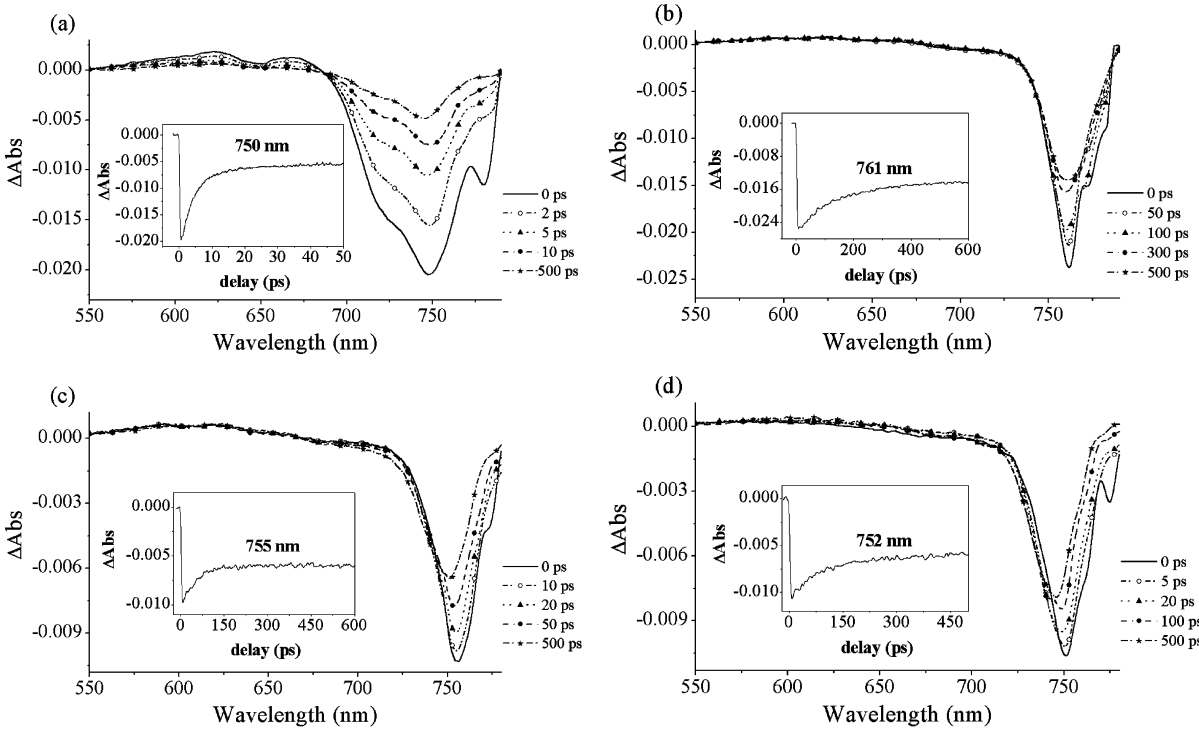

Figure 4. Time-resolved spectra of WST11 in (a) PBS, (b) PBS + 150 μM HSA, (c) MeOH, and (d) AN. The measurements were carried out under anaerobic conditions. Data collection time was 45 min per transient.

position in PBS and peak at 744 and 514 nm, respectively, while the B_x and B_y slightly red-shifted and peak at 383 and 326 nm, respectively. The electrochemical oxidation induces bleaching of the major transition bands of WST11 at 382, 514, and 744 nm and an absorption increase at 448, 548, and 821 nm, where the latter is the most prominent transition band. Upon the back reduction process, the bleaching of these bands allows their assignment to the cationic $WST11^+$. The electrochemical reduction results in a similar bleaching pattern but a significantly different absorption increase, with major transitions at 411 (strong) and 824 (weak) nm (Figure 3b). The reaction reversibility is ~50% and ~30% for the oxidation and reduction processes, respectively. The rest of the compound was irreversibly degraded to the bacteriochlorine form, indicated by the transition band at ~640 nm.[24,30,32,33]

Time-Resolved Changes in the Optical Absorption of WST11 in Response to Pulsed Illumination at the Femto- to Picosecond Time Domain. Figure 4 illustrates the ultrafast response of 25 μM WST11 in different solutions to 120 fs light pulses at 525 nm (pump pulse energy 2.3 μJ, which did not induce significant degradation after several measurement sets). The corresponding kinetic parameters of the transient absorption and bleaching recovery are given in Table 1.

The 750 nm absorption and the accompanying shoulder at 715 nm undergo instantaneous bleaching. The bleaching is accompanied by an absorption increase at 585, 625, and 670 nm. Between 10 and 15 ps, about 75% of the bleached spectrum recovers, and the transient absorption decays to a longer-living state (at 585 nm, Figure 4a), at a rate of 1.2×10^{11} s^{-1} (Table 1). In the presence of HSA (Figure 4b), the absorption in the Q_y domain bleaches as a single band (in agreement with the proposed monomerization of the compound),[14] and 20% of the bleached spectrum recovers at a rate of 4.5×10^{10} s^{-1} (Table 1). An additional 10% recovers at a rate of 6.6×10^9 s^{-1} (Figure 4b and Table 1). The rest appears as a long-living state that decays in the nano/millisecond time domain (see below), fairly similar to the yield and decay rate of the long-living excited form of WST09.[24] The transient absorption and bleaching of WST11 in response to the 120 fs pulses in MeOH and AN (Figure 4c and d, respectively) appear similar to those observed in the HSA solutions, but the corresponding rate constants for 30% recovery are about half (2×10^{10} s^{-1}, Table 1). Importantly,

TABLE 1: Kinetic Parameters of the Transient Absorption and Bleaching Recovery of WST11 in Different Solutions

	WST11 in PBS				
	585 nm[a,b]	625 nm[a,b]	670 nm[a,b]	715 nm[b]	750 nm[b]
τ (ps) [k (1/s)]	7.9 ± 2 [1.2×10^{11}]	5.2 ± 0.5 [1.9×10^{11}]	4.7 ± 0.4 [2×10^{11}]	5.4 ± 0.1 [1.8×10^{11}]	4.8 ± 0.1 [2×10^{11}]
R^2	0.32	0.66	0.70	0.99	0.99

	WST11 in PBS + 150 μM HSA	WST11 in MeOH	WST11 in AN
	761 nm[b]	755 nm[b]	752 nm[b]
τ (ps) [k (1/s)]	24 ± 11, 152 ± 6 [4.5×10^{10}, 6.6×10^{9}]	50 ± 3 [2×10^{10}]	50 ± 13, 226 ± 75 [2×10^{10}, 4.4×10^{9}]
R^2	0.98	0.79	0.96

[a] Absorption band. [b] Bleaching.

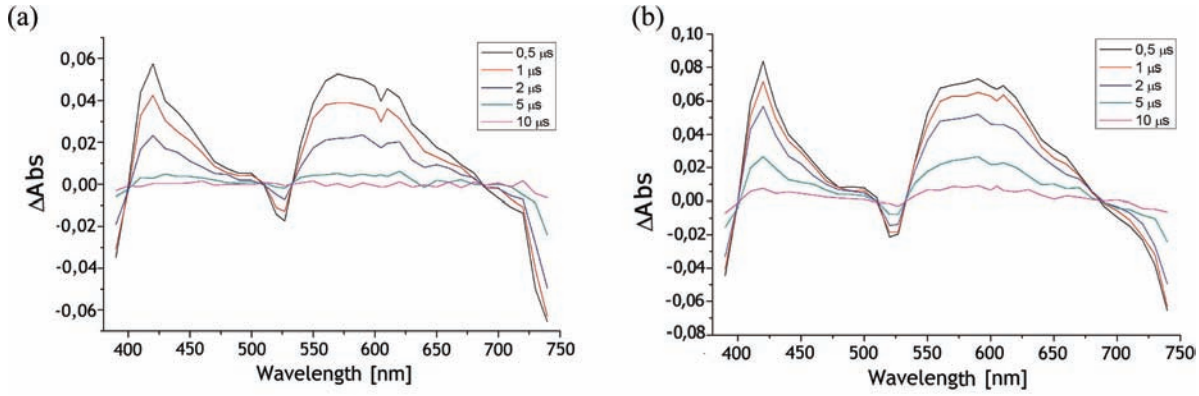

Figure 5. Time-dependent changes in optical absorption of 25 μM WST11 + 150 μM HSA in PBS after 532 nm pulsed excitation (5 ns pulse duration). (a) Oxygen-saturated solution; (b) argon-saturated solutions. During this experiment, total exposure time to white monitoring light did not exceed 5 s. Each data point was obtained by a single laser flash (energy ~1.5 mJ).

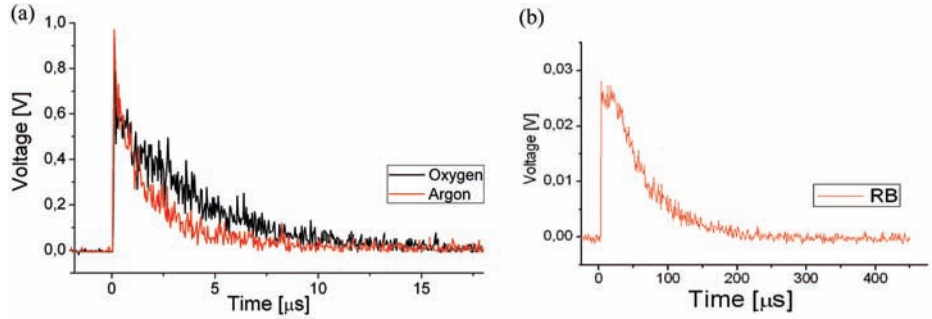

Figure 6. (a) The 1272 nm emission due to a single, 5 ns flash excitation at 532 nm of WST11/HSA/D2O solution saturated with argon (red line) or molecular oxygen (black line). (b) The 1272 nm emission due to excitation of Rose Bengal in oxygen-saturated solutions.

the transient absorption of WST11 in PBS features peaks between 500 and 700 nm (Table 1). This can be carefully attributed to the cationic form of WST11 as derived from Figure 3a, with some red shift that reflects the solvent effect.

Measurements at the Sub-microsecond to Millisecond Time Domain. Figure 5 presents the long-living transient optical absorption of WST11 in PBS\HSA solutions, under oxygen or argon saturation, from the submicro- to the millisecond time range.

While the two spectra appear similar, saturation with argon gives rise to an absorption increase at 605 nm that partly bleaches during the first microsecond after excitation in the oxygen-saturated solutions. Although the difference between the ground and long-living excited state of WST11 resembles the one observed for WST09,[24] there are several profound differences. First, WST11 presents transient absorption at 418 nm that is several times stronger than the absorption of WST09 at this wavelength region. Second, the VIS absorption of WST11 includes shoulders that extend beyond 605 nm, whereas WST09 presents a single absorption increase at 575 nm. To gain a better insight into the origin of the long-living transient absorption, we examined the NIR emission of WST11 in PBS/HSA solution under argon or oxygen saturation. The results are presented in Figure 6a.

Typical to both Bchl triplets is the fairly strong emission (phosphorescence) at ~1160−70 nm that extends up to 1272 nm.[24,39] This emission can overlap the emission of singlet oxygen.[24,39] Thus, the 1272 nm emission of aerobic solutions of Bchl derivatives can be contributed by both the Bchl triplet state and photodynamically generated singlet oxygen molecules. Fortunately, the decay rate of the Bchl phosphorescence is larger by more than an order of magnitude than the singlet oxygen decay in D_2O solutions, thus enabling good resolution of the two.[24] Table 2 summarizes the corresponding kinetic parameters.

TABLE 2: Kinetic Parameters of WST11 Transient Absorption at the Sub-microsecond to Millisecond Time Domain

	oxygen-saturated solution	argon-bubbled solution
τ (μs) [k (1/s)]	1.72 [5.8×10^5]	4.22 [2.4×10^5]
standard error	0.04	0.13

The phosphorescence signal in the argon-saturated solution decays at a rate of 2.4×10^5 s^{-1} and at a double rate of 5.8×10^5 s^{-1} in the oxygen-saturated solution. No significant change in the signal amplitude was observed in the presence of oxygen. Figure 6b illustrates the decay of the 1272 nm emission (excitation at 532 nm) generated by Rose Bengal in PBS/HSA/D_2O solution that have the same OD at 532 nm. The rate constant of the 1272 nm generated by Rose Bengal, which is uniquely identified with singlet oxygen emission, is by far smaller (0.1×10^5 s^{-1}), as we previously reported.[24] Cumulatively, our data exclude the formation of singlet oxygen by photoexcited WST11 in aqueous solutions. In the absence of singlet oxygen generation, only $OH^\bullet$ and $O_2^{-\bullet}$ radicals can be generated by the photoexcited WST11. To better identify the evolved ROS, we utilized the ESR technique.

Generation of ROS by Photoexcited WST11 in the Absence of Serum Albumin. Figure 7 shows the ESR spectra of the photogenerated and spin-trapped $OH^\bullet$ and $O_2^{-\bullet}$ radicals upon illumination of WST11 in PBS solution, using DMPO as the spin trap.

Verifying the Genuine Production of $O_2^{-\bullet}$ and $OH^\bullet$ Radicals. A shortcoming of using DMPO as a spin trap is the rapid decomposition of the DMPO−OOH adduct to DMPO−OH. To overcome this problem and to verify the production of a genuine $OH^\bullet$ radical in our system, we used the selective 5-diethoxyphosphoryl-5-methyl-1-pyrroline *N*-oxide (DEPMPO) spin-trap, as previously described.[24] The DEPMPO−OOH adduct does not degrade to the DEPMPO−OH adduct, therefore allowing selective trapping of $OH^\bullet$ and $O_2^{-\bullet}$ radicals. Figure 8 presents the experimental and corresponding simulated ESR signals of the DEPMPO−OOH and DEPMPO−OH spin adducts, obtained upon illumination of WST11 in PBS.

This result confirms that WST11 produces both $OH^\bullet$ and $O_2^{-\bullet}$ radicals in aqueous solutions. The concentrations of the photogenerated radicals were calculated using the following equations:

$$[OH^\bullet] = \frac{S_{DEPMPO-OH}}{S_{stn}}[stn] \text{ and } [O_2^{-\bullet}] = \frac{S_{DEPMPO-OOH}}{S_{stn}}[stn]$$

In these expressions, $S_{DEPMPO-OH}$ and $S_{DEPMPO-OOH}$ are the integrated ESR signal of DEPMPO−OH and DEPMPO-OOH, respectively. S_{stn} is the integrated ESR signal of a standard ([3-carboxy-PROXYL]). Accordingly, the obtained concentration values for the $OH^\bullet$ and $O_2^{-\bullet}$ radicals are 5 and 10 μM, respectively. The number of radicals generated in the entire experimental volume V is

$$N_{OH^\bullet} = N_A[OH^\bullet]V = 1.5 \times 10^{14} \text{ and } N_{O_2^{-\bullet}} = N_A[O_2^{-\bullet}]V = 3.0 \times 10^{14}$$

where N_A is the Avogadro number and $V = 50$ μL. The energy needed to generate these radicals, 2.4 J, was delivered by 9×10^{18} photons at 755 nm through an optical path of 0.2 cm. Using eq 13 in Vakrat et al.[24] for 100 μM WST11, and assuming a similar cross section of absorption for WST11 and WST09 (1.2×10^{-16} cm^2), we found that the delivered energy could generate 5×10^{17} WST11 molecules in the excited triplet state (e.g., under anaerobic conditions). Figure 4b shows that ~70% of WST11 molecules that were excited to their first excited singlet state (in one 120 fs pulse) relaxed into their triplet state. Upon collision with ground-state oxygen, ~66% of the formed complexes (i.e., those having a spin multiplicity of 1) can make ion pairs.[40,41] Thus, the apparent quantum yield of $O_2^{-\bullet}$ and $OH^\bullet$ radicals can reach $4.5 \times 10^{14}/2.3 \times 10^{17} \sim 2 \times 10^{-3}$ or 0.2% in the PBS solution (using eq 14 in Vakrat et al.).[24] However, each oxidized WST11 undergoes irreversible degradation under aerobic conditions and in the absence of compensating reducing agents, as previously explained for WST09.[24] Following these constraints, the integrated number of the photoexcited WST11 molecules in the singlet state is significantly reduced, and the quantum yield for radical formation should be markedly higher than the above value. Indeed, such higher yields are demonstrated below in the presence of HSA.

Generation of ROS by Photoexcited WST11 in the Presence of Human Serum Albumin. Figure 9 shows the effect of HSA on $OH^\bullet$ radical generation by WST11 upon consecutive illumination−reoxygenation cycles in the presence and absence of HSA.

The sample (1 mL of 100 μM WST11) was placed in an optical cuvette of 0.5 cm path length where it was periodically illuminated for 2 min at 755 nm (20 mW). After each illumination period, an aliquot of 50 μL was examined by ESR while the sample in the cuvette was introduced to a stream of oxygen under dark conditions until saturation of dissolved oxygen was reached. This light−dark−reoxygenation cycle was repeated until the complete degradation of the WST11−HSA complex (monitored spectroscopically as in Figure 1b). After the first period of illumination, the concentration of DMPO−OH

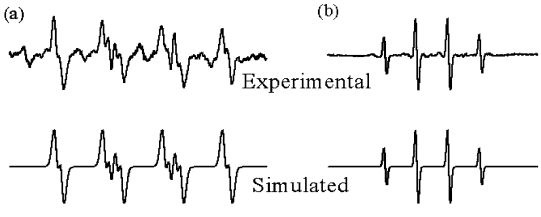

Figure 7. ESR spectra of the photogenerated ROS upon illumination of WST11 (100 μM) at 755 nm (20 mW, 2 min) in PBS. (a) Signal of DMPO−OOH. The signal was acquired in the presence of 10% DMSO used as an $OH^\bullet$ radical quencher. Simulation parameters: $a_N = 13.98$, $a_{H\beta} = 11.26$, $a_{H\gamma} = 1.27$, $R = 0.91$. (b) Signal of DMPO−OH; simulation parameters: $a_N = 14.88$, $a_H = 14.68$, $R = 0.99$. DMPO concentration was 80 mM.

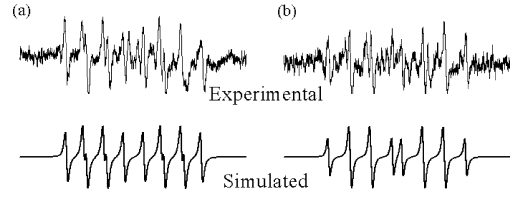

Figure 8. ESR spectra of DEPMPO−OOH and DEPMPO−OH adducts obtained upon illumintion of WST11 (100 μM) at 755 nm (20 mW, 2 min). (a) Signal of DEPMPO−OOH. The signal was acquired in the presence of 10% DMSO used as an $OH^\bullet$ radical quencher. Simulation parameters: $a_p = 50.3$ G, $a_N = 13.8$ G, $a_H = 11.1$ G. (b) Signal of DEPMPO−OH, obtained by subtracting the pure DEPMPO−OOH signal from the original mixed signal. Simulation parameters: $a_p = 47.0$ G, $a_N = 13.5$ G, $a_H = 14.0$ G. DEPMPO concentration was 170 μM.

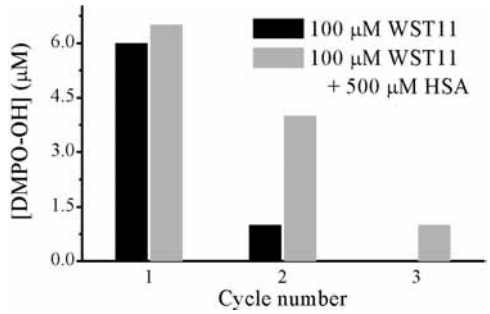

Figure 9. Effect of HSA (500 μM) on the photogeneration of OH$^{\bullet}$ radical by WST11 (1 mL of 100 μM WST11 in PBS, placed in an optical cuvette). The sample was illuminated periodically for 2 min at 755 nm (20 mW). After each illumination period, an aliquot of 50 μL was examined by ESR, while the cuvette was introduced to a stream of molecular oxygen. This was repeated until the complete degradation of the WST11−HSA complex (monitored spectroscopically).

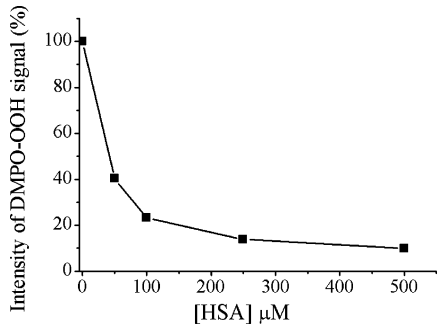

Figure 10. Effect of HSA on the DMPO−OOH ESR signal. [WST11] = 100 μM, [DMPO] = 80 mM. Illumination was performed for 10 min at 755 nm (20 mW).

reached a fairly similar level as in the sample that did not contain HSA. However, after a second period of illumination, in the absence of HSA the concentration of DMPO−OH decreased by 85% relative to the first illumination period, whereas in the presence of HSA, the concentration decreased only by 40%. In the third cycle, no radicals were produced in the non-HSA solution, while in the presence of HSA, OH$^{\bullet}$ radicals were produced at 15% of the initial yield. Altogether, the concentration of the trapped OH$^{\bullet}$ radical increased by more than 2-fold in the presence of HSA, reaching a total value of 12 μM under the applied experimental conditions.

Figure 10 shows that addition of HSA quenched the spin-trapped $O_2^{\bullet}$ to about 10% of its value in the absence of HSA.

The addition of oxygen and the application of periodic illumination as described above did not affect the concentration of the DMPO−OOH adduct. These findings suggest that either the generation of $O_2^{-\bullet}$ radicals is significantly lowered in the presence of HSA or that the radicals rapidly interact with the protein.

Effect of HSA on Oxygen Consumption during WST11 Illumination in Aqueous Solutions. Generation of reactive oxygen species upon illumination of WST11 is accompanied by rapid consumption of molecular oxygen. In fact, we have recently found that this is an important part of the VTP mechanism in vivo.[42] Hence, we independently explored the consumption of molecular oxygen under illumination of WST11−HSA solutions. Figure 11a (left side) shows that in the absence of HSA molecular oxygen is consumed at a rate of 0.23 μM s^{-1} and levels off after 11 min of illumination. At that time, WST11 undergoes complete bleaching and is converted into a bacteriochlorine type molecule (Figure 11a, right side). Figure 11b (left side) shows that upon adding HSA to WST11/PBS solution the light-induced consumption of molecular oxygen is significantly enhanced in terms of kinetics and yield. Under these conditions, 20 min of illumination brought about the complete depletion of 270 μM of dissolved molecular oxygen at a rate of 0.86 μM s^{-1}. Yet, only ∼30% of the WST11−HSA complex has been degraded (Figure 11b, right side). Oxygen replenishment of the solution to the level of saturation during a short dark period (15 s) followed by 6.5 min of illumination resulted in the consumption of additional 270−300 μM molecular oxygen at a rate of 1.7 μM s^{-1} (Figure 11c, left side) and additional 30% degradation of WST11 (Figure 11c, right side). An additional oxygen replenishment and illumination of the sample ended after 4.5 min with another depletion of 230 μM molecular oxygen at a rate of 2.15 μM s^{-1} (Figure 11d, left side) and the complete degradation of the WST11−HSA (Figure 11d, right side).

Altogether, 750−800 compared to 50 μM of molecular oxygen was consumed upon illumination of 100 μM WST11 in the presence and absence of HSA, respectively.

Quantum Yield for Oxygen Consumption by WST11 in Aqueous Solutions Containing HSA. Using the second and third cycles, we calculated the apparent quantum yield for oxygen consumption by light-excited WST11. The linear consumption of oxygen in each of these cycles continued for ∼60 s during which 4.5×10^{18} photons at 755 nm were delivered. This delivery generated 1.3 μM of OH$^{\bullet}$ radicals (Figure 9) and consumed 150 μM of molecular oxygen (Figure 11c and d). Since the calculated quantum yield for OH$^{\bullet}$ generation by WST11 in the excited triplet state is 0.2% (see above), the calculated quantum yield for oxygen consumption by this compound in the presence of HSA is 21%, one-third of the upper limit expected (assuming a charge transfer mechanism that involves the spin 1 multiplicity of the collision complex between molecular oxygen and WST11 at the excited triplet state).[40,41] Since no singlet oxygen could be detected both in the absence (data not shown) and in the presence of HSA (Figure 6), we can conclude that the oxygen consumption involved only reduction by the noncovalent WST11−HSA complexes. However, since only 1.3 μM of such radicals was trapped, the rest should interact with the protein molecules.

Oxidation of HSA by ROS, Generated through Excitation of WST11−HSA Noncovalent Complexes. Although both oxygen consumption and spin-trapped radical concentrations are increased upon adding HSA to the WST11 solutions, the former is ∼15 times higher than the latter. At the same time, the photochemical degradation of WST11 is dramatically attenuated. Thus, the value of [consumed WST11]/[consumed O_2] is 1.5 and 0.1 in the absence and presence of HSA, respectively. Still, there is no apparent difference in the overall concentration of spin-trapped ROS ($O_2^{-\bullet}$ and OH$^{\bullet}$) in the two examined solutions. This discrepancy prompted us to look for possible interactions of the photogenerated ROS with the HSA molecules.

Reactions of ROS with serum proteins are common in biological contexts; the oxidation of Trp residues by ROS is the most commonly reported pathway.[43,44] Moreover, interaction of singlet oxygen with HSA during PDT with porphyrins has been reported.[45] Nevertheless, to the best of our knowledge, this interaction has never been quantified. Peroxidation of serum proteins may slightly increase their molecular weight and/or drive cross-link formation between several HSA monoproteins. The above should result in mass changes that can be monitored by gel electrophoresis if large enough or by mass spectrometry if the peroxidation involves small changes.

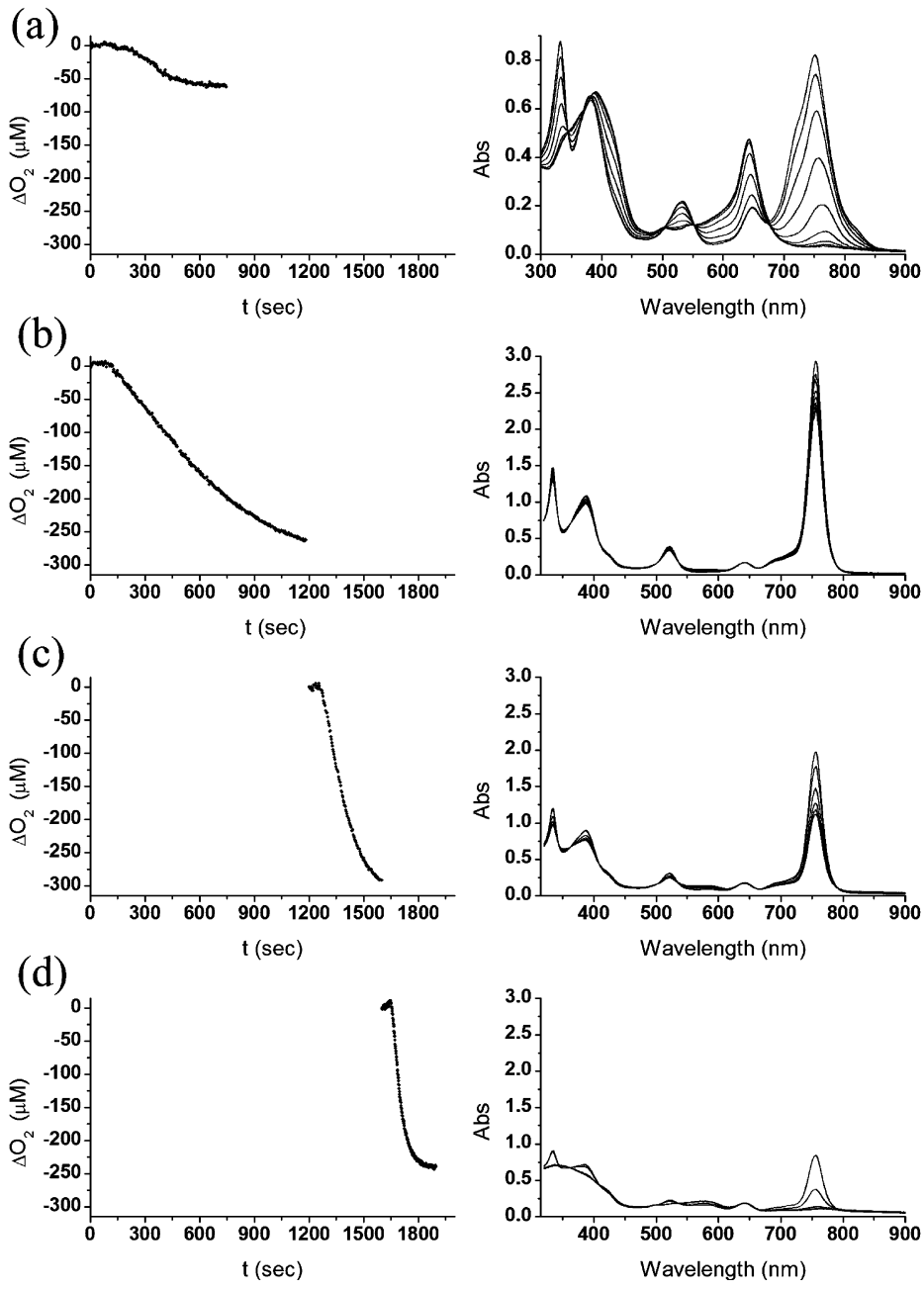

Figure 11. Light-induced oxygen consumption of WST11 (100 μM) during illumination at 755 nm (20 mW) and the corresponding spectral evolution: (a) oxygen consumption during 11 min illumination of WST11 in the absence of HSA; (b) first cycle of oxygen consumption in the presence of HSA (500 μM) and 20 min of illumination; (c) second cycle of light-induced oxygen consumption: after cycle b ended, the solution was replenished by oxygen (dark period of 15 s) and then illuminated for a period of 6.5 min; (d) additional cycle of light-induced oxygen consumption: following the ending of cycle c, the solution was replenished by oxygen (dark perdion of 15 s) and then illuminated for a period of 4.5 min.

Gel electrophoresis of HSA collected from samples of WST11 after extensive illumination did not reveal any significant cross-link formation (not shown). However, ESI−mass spectrometry of HSA before and after PDT was monitored revealed a mass increase of 224 g/mol (Figure 12) in the HSA fraction that was bound to WST11 during illumination (collected as the colored fraction).[14]

This additional mass corresponds to seven molecules of oxygen added to each molecule of HSA during the entire period of illumination. Since more than 90% of the WST11 molecules are bound in a 1:1 complex with HSA, the WST11−HSA concentration is ~100 μM, accounting for ~700 μM out of the 750−800 μM of consumed oxygen molecules.

Unfortunately, we were not able to isolate and directly identify the affected residues; however, HSA contains a single tryptophan (Trp) that was involved in different redox reactions with attached ligands[46,47] and is close to one of the putative porphyrin binding sites in HSA. To determine whether this Trp residue is close to the bound WST11, we followed its fluorescence at different relative HSA and WST11 concentrations, both in aerobic and anaerobic solutions (after extensive purging with argon). To avoid any fluorescence admixing from the multiple Tyr residues in the HSA scaffold, excitation was performed at 295 nm which is sufficiently far from Tyr absorption at 280 nm (as recently reported by Rolinsky et al.[48] and previously suggested by Lakowitz[49]) using narrow slits. As illustrated in Figure 13,

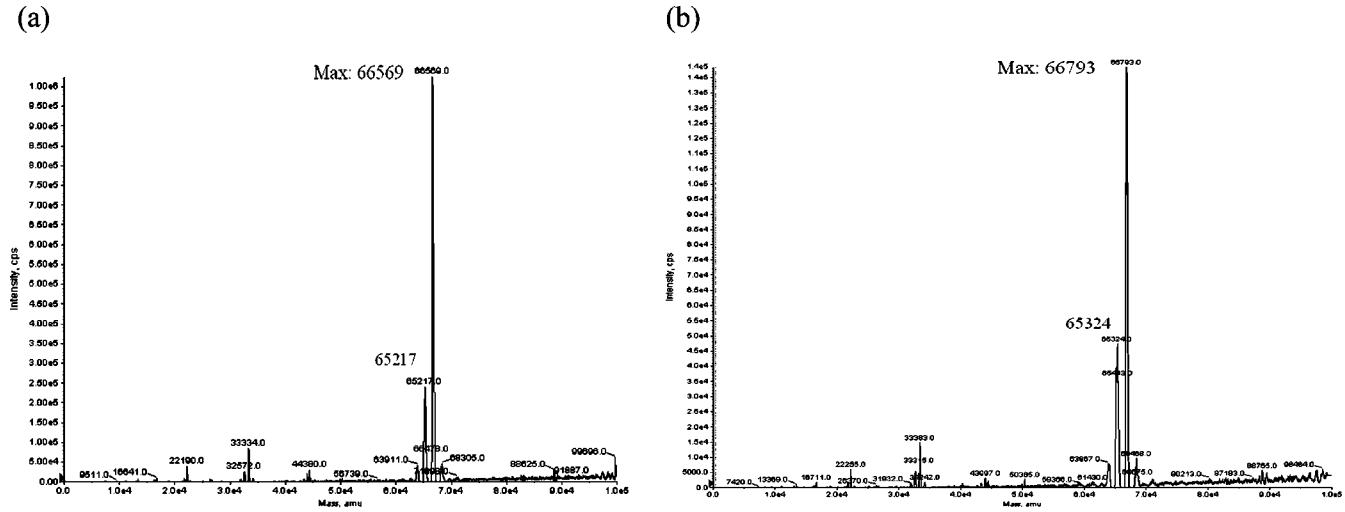

Figure 12. ESI−MS spectra of HSA before (a) and after (b) the introduction of WST11 in PBS. The analysis was done after illumination of the samples at 755 nm (20 mW, 10 min).

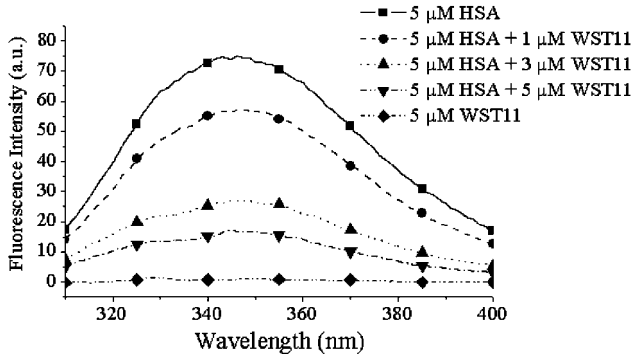

Figure 13. Fluorescence of the HSA's tryptophan residue at different concentrations of WST11. λ_{Ex}, 295 nm; λ_{Em}, 310−400 nm. [HSA] = 5 μM.

we could clearly monitor the quenching of the fluorescence of this Trp residue upon adding WST11 regardless of the oxygen content, suggesting energy transfer to the very weakly NIR fluorescing WST11.

We therefore propose that WST11 is bound at a close distance to the Trp and that part of the generated radicals interact with this residue. This hypothesis as well as the search for other specific interactions is currently under investigation in our group (see Discussion below).

Discussion

In this study, we monitored ROS photogeneration by WST11 in buffered aqueous solutions with no added amphiphilic agents. Specifically, we examined the effect of HSA, the major carrier of WST11 in the circulation and a well-recognized antioxidant agent,[50−55] on the profile and dynamics of the photogenerated ROS as well as regarding the details of the concomitant oxygen consumption. We showed that in both the absence and presence of HSA the primary photogenerated ROS are $O_2^{-\bullet}$ and $OH^{\bullet}$ radicals with no detectable singlet-oxygen generation. This observation infers that WST11−VTP, where the sensitizer is illuminated in the lumen as a WST11−HSA noncovalent complex, is most probably mediated by type I (electron transfer) and not type II (energy transfer) processes. In PBS solutions, oxygen consumption and the related generation of $OH^{\bullet}$ and $O_2^{-\bullet}$ radicals were accompanied by consumption and degradation of a similar number of WST11 molecules. In contrast, upon adding HSA (at physiological concentrations), each molecule of WST11 drove the consumption of 8−9 molecules of oxygen before degradation by radical formation. Since each molecule of WST11 can provide only 1−2 electrons upon monochromatic excitation before undergoing oxidative degradation, additional electrons had to be provided, most probably from the HSA proteins that underwent complexation with WST11. This suggests that WST11 photocatalyzed the electron transfer from the bound HSA molecule into the colliding oxygen molecules through several cycles. As Figure 3 illustrates, both the cation and anion of WST11 are fairly stable and can participate in reversible redox reactions. If electrons are rapidly provided, minimal degradation occurs. Thus, we propose that electron transfer from the excited WST11 (noncovalently bound to HSA) to a colliding oxygen molecule is immediately followed by a compensating electron transfer to the formed $WST11^{+}$ cation species. Overall, such oxidation and compensating reduction should result in only small changes of the ground-state absorption (Figure 3, considering the irreversible degradation to the oxidized form of WST11 as depicted by the 640 nm transition band) but should accelerate the decay of the excited triplet state, as obtained here (Table 2 and Figures 5 and 6). There are several possible sources for the electrons provided by the HSA. Bound metals such as Fe^{2+} or Cu^{1+} are one such source. However, addition of the metal chelator desferroxamine[56] (20 mM) to the PBS/HSA solution did not reduce neither the rate nor the amount of oxygen consumption, and although the amount of trapped $OH^{\bullet}$ radicals reduced, it was adequately compensated by a steep concentration increase of trapped $O_2^{-\bullet}$ radicals (data not shown). Thus, amino acid residues of the binding HSA are the most likely providers of the electrons.[46] The oxidized HSA can undergo immediate nucleophilic reduction by the generated $O_2^{-\bullet}$ radicals but not by the $OH^{\bullet}$ radicals. Additionally, the $O_2^{-\bullet}$ radicals can oxidize different residues of the HSA such as the nearby tryptophan, cystein, tyrosine, and methionin side chains. In this regard, the well-recognized antioxidative activity of HSA is most relevant.[50−55] Several such cycles should result in significant generation of $OH^{\bullet}$ radicals but minimal traces of $O_2^{-\bullet}$ species.

Conclusions

An excited WST11 molecule, noncovalently bound to the HSA skeleton, can transfer an electron to molecular oxygen to form the $O_2^{-\bullet}$ radical. In turn, the bound $WST11^{+}$ cation accepts an electron from an HSA residue. This cyclic light-induced process proceeds until the protein loses its capacity to donate electrons as a result of extensive peroxidation in agreement with the observed HSA

damage. This finding and the accompanied detailed analysis suggest that WST11−HSA can be regarded as a simple reaction center unit that photocatalyzes oxidoreductive reactions as needed for ROS generation in VTP. Other evidence supporting the capacity of HSA as an electron donor to different photoexcited molecules was recently published.[46] However, we are not aware of any evidence of a two-step process like the one suggested here. In view of our findings, it is expected that under fractionated light and in the presence of agents that can rapidly reduce the oxidized HSA, the ROS yield may be highly increased, having clear clinical implications and ramifications.

Furthermore, the regeneration of the WST11 photocatalytic redox center by electron mobilization from the protein closely resembles the regeneration of the active primary donors in PSII RC and genetically engineered RC of purple bacteria as reviewed in the Introduction. Thus, further studies of the presented HSA/WST11 and similar systems is expected to shed light on the development of the light conversion machinery in biological photosynthesis and artificial systems.

Acknowledgment. A.S. and Y.S. are the incumbents of the Robert and Yaddele Sklare Professorial Chair in Biochemistry and the Tillie and Charles Lubin Professorial Chair in Biochemical Endocrinology, respectively. I.A. and R.G. have equally contributed to this study. WST11 was prepared by STEBA LABORATORIES (Israel). Transient absorption studies were performed at the Dr. J. Trachtenberg laboratory for photobiology and photobiotechnology (The Weizmann Institute). We are grateful to Prof. E. Riedle, from LMU, Munich, Germany, for helping us in designing the white light generator for the femto−picosecond experiment. The study was supported by research grants from STEBA-BIOTECH (France) and from Sharon Zuckerman (Toronto, Canada) and by the Ministry of Science and Higher Education (DS 4.1.874, Poland).

References and Notes

(1) Moser, C. C.; Page, C. C.; Chen, X.; Dutton, P. L. *Subcell. Biochem.* **2000**, *35*, 1.
(2) Beretan, D. N.; Onuchic, J. N. *Protein Electron Transfer*; Bios Scientific Publishers: Oxford, 1996.
(3) Takahashi, S.; Murata, N. *Trends Plant Sci.* **2008**, *13*, 178.
(4) Battle, A. M. D. *Photochem. Photobiol. B* **1993**, *20*, 5.
(5) McCaughan, J. S. *Drugs & Aging* **1999**, *15*, 49.
(6) Silva, A. R. d.; Ribeiro, J. N.; Rettori, D.; Jorge, R. A. *J. Braz. Chem. Soc.* **2008**, *19*, 1311.
(7) Foote, C. S. *Am. Chem. Soc. Symp. Ser.* **1987**, *339*, 22.
(8) Wilkinson, F.; Brummer, J. G. *J. Phys. Chem. Ref. Data* **1981**, *10*, 809.
(9) Jori, G. *Lasers in Photomedicine and Photobiology*; Springer-Verlag: Berlin, 1980; Vol. 22.
(10) Rossi, E.; Vandevorst, A.; Jori, G. *Photochem. Photobiol.* **1981**, *34*, 447.
(11) Skalkos, D.; Hampton, J. A.; Keck, R. W.; Wagoner, M.; Selman, S. H. *Photochem. Photobiol.* **1994**, *59*, 175.
(12) Solban, N.; Rizvi, I.; Hasan, T. *Lasers Surg. Med.* **2006**, *38*, 522.
(13) Solban, N.; Selbo, P. K.; Sinha, A. K.; Chang, S. K.; Hasan, T. *Cancer Res.* **2006**, *66*, 5633.
(14) Brandis, A.; Mazor, O.; Neumark, E.; Rosenbach-Belkin, V.; Salomon, Y.; Scherz, A. *Photochem. Photobiol.* **2005**, *81*, 983.
(15) Mazor, O. Synthesis of Phototoxicity of Novel Sulfonated Bacteriochlorophyll Derivatives. Ph.D., The Weizmann Institute of Science, 2004.
(16) Mazor, O.; Brandis, A.; Plaks, V.; Neumark, E.; Rosenbach-Belkin, V.; Salomon, Y.; Scherz, A. *Photochem. Photobiol.* **2005**, *81*, 342.
(17) Berdugo, M.; Bejjani, R. A.; Valamanesh, F.; Savoldelli, M.; Jeanny, J.; Blanc, D.; Ficheux, H.; Scherz, A.; Salomon, Y.; Ben-Ezra, D.; Behar-Cohen, F. *Invest. Ophthalmol. Visual Sci.* **2008**, *49*, 1633.
(18) Gross, S.; Gilead, A.; Scherz, A.; Neeman, M.; Salomon, Y. *Nat. Med.* **2003**, *9*, 1327.
(19) Lepor, H. *Rev. Urol.* **2008**, *10*, 254.
(20) Trachtenberg, J.; Bogaards, A.; Gertner, M.; Weersink, R. A.; Yue, C.; Scherz, A.; Savard, J.; Evans, A.; McLusky, S.; Haider, M. A.; Aprikian, A.; Wilson, B. C.; Elhilali, M. *J. Urol.* **2007**, *178*, 1974.
(21) Trachtenberg, J.; Weersink, R. A.; Davidson, S. R. H.; Haider, M. A.; Bogaards, A.; Gertner, M. R.; Evans, A.; Scherz, A.; Savard, J.; Chin, J. L.; Wilson, B. C.; Elhilali, M. *BJU International*, **2008**, *102*, 556.
(22) Eggener, S. E.; Coleman, J. A. *ScientificWorldJournal* **2008**, *8*, 963.
(23) MacDonald, I. J.; Dougherty, T. J. *J. Porphyrins Phthalocyanines* **2001**, 5.
(24) Vakrat-Haglili, Y.; Weiner, L.; Brumfeld, V.; Brandis, A.; Salomon, Y.; McIlroy, B.; Wilson, B. C.; Pawlak, A.; Rozanowska, M.; Sarna, T.; Scherz, A. *J. Am. Chem. Soc.* **2005**, *127*, 6487.
(25) Brun, P. H.; DeGroot, J. L.; Dickson, E. F. G.; Farahani, M.; Pottier, R. H. *Photochem. Photobiol. Sci.* **2004**, *3*, 1006.
(26) Grabolle, M.; Dau, H. *Biochim. Biophys. Acta* **2005**, *1708*, 209.
(27) Tommos, C.; Babcock, G. T. *Biochim. Biophys. Acta* **2000**, *1458*, 199.
(28) Kalman, L.; Williams, J. C. *Photosynth. Res.* **2008**, *98*, 643.
(29) Halliwell, B.; Gutteridge, J. M. C. ESR and spin trapping. In *Free Radicals in Biology and Medicine*; Oxford University Press: Oxford, UK, 1999; p 357.
(30) Gouterman, M. *J. Mol. Spectrosc.* **1961**, *6*, 138.
(31) Gouterman, M.; Wagniere, G. H. *J. Mol. Spectrosc.* **1963**, *11*, 108.
(32) Scherz, A.; Roshenbach-Belkin, V.; Fisher, J. R. E. In Chlorophylls. In *chlorophylls*; CRC Press: Boca Raton, 1991; p 273.
(33) Hanson, L. K. In Chlorophylls. In *chlorophylls*; CRC Press: Boca Raton, 1991; p 993.
(34) Scherz, A.; Parson, W. W. *Biochim. Biophys. Acta* **1984**, *766*, 653.
(35) Scherz, A.; Rosenbachbelkin, V. *Proc. Natl. Acad. Sci. U.S.A.* **1989**, *86*, 1505.
(36) Scherz, A.; Parson, W. W. *Biochim. Biophys. Acta* **1984**, *766*, 666.
(37) Noy, D.; Fiedor, L.; Hartwich, G.; Scheer, H.; Scherz, A. *J. Am. Chem. Soc.* **1998**, *120*, 3684.
(38) Geskes, C.; Hartwich, G.; Scheer, H.; Mantele, W.; Heinze, J. *J. Am. Chem. Soc.* **1995**, *117*, 7776.
(39) Hartwich, G.; Fiedor, L.; Simonin, I.; Cmiel, E.; Schafer, W.; Noy, D.; Scherz, A.; Scheer, H. *J. Am. Chem. Soc.* **1998**, *120*, 3675.
(40) Dzhagarov, B. M.; Sagun, E. I.; Ganzha, V. A.; Gurinovich, G. P. *Khim. Fiz.* **1987**, *6*, 919.
(41) Dzhagarov, B. M.; Gurinovich, G. P.; Novichenkov, V. E.; Salokhiddinov, K. I.; Shulga, A. M.; Ganzha, V. A. *Khim. Fiz.* **1987**, *6*, 1069.
(42) Madar-Balakirski, N.; Tempel-Brami, C.; Kalchenko, V.; Scherz, A.; Salomon, Y. Submitted to the *Int. J. Cancer*.
(43) Dyer, J. M.; Bringans, S. D.; Bryson, W. G. *Photochem. Photobiol.* **2006**, *82*, 551.
(44) Dyer, J. M.; Bringans, S. D.; Bryson, W. G. *Photochem. Photobiol.* **2006**, *5*, 698.
(45) Korinek, M.; Dedic, R.; Molnar, A.; Hala, J. *J. Fluoresc.* **2006**, *16*, 355.
(46) Kobori, Y.; Norris, J. R., Jr. *J. Am. Chem. Soc.* **2006**, *128*, 4.
(47) Davies, K. J. A.; Lin, S. W.; E., P. R. *J. Biol. Chem.* **1987**, *262*, 9914.
(48) Rolinski, O. J.; Martin, A.; Birch, D. J. S. *Ann. N.Y. Acad. Sci.* **2008**, *1130*, 314.
(49) Lakowicz, J. R. *Principles of Fluorescence Spectroscopy*; Plenum Press: New York, 1986.
(50) Cao, G.; Prior, R. L. *Clin. Chem.* **1998**, *44*, 1309.
(51) Jennifer, A.; Irwin, H.; Davies, M. J. *Arch. Biochem. Biophys.* **1999**, *362*, 94–104.
(52) Faure, P.; Tamisier, R.; Baguet, J. P.; Favier, A.; Halimi, S.; Levy, P.; Pepin, J. L. *Eur. Respir. J.* **2008**, *31*, 1046.
(53) Cha, M. K.; Kim, I. H. *Biochem. Biophys. Res. Commun.* **1996**, *222*, 619.
(54) Wayner, D. D.; Burton, G. W.; Ingold, K. U.; Locke, S. *FEBS Lett.* **1985**, *187*, 33.
(55) Armstrong, J. S.; Rajasekaran, M.; Hellstrom, W. J.; Sikka, S. C. *J. Androl.* **1998**, *19*, 412.
(56) Halliwell, B.; Gutteridge, J. M. C. Iron chelators. In *Free Radicals in Biology and Medicine*; Oxford University Press: Oxford, UK, 1999; p 843.

JP900580E